V-Pits and Trench-Like Defects in High Periodicity MQWs GaN-Based Solar Cells: Extensive Electro-Optical Analysis

Marco Nicoletto, *Student Member, IEEE*, Alessandro Caria, Fabiana Rampazzo, Carlo De Santi, *Member, IEEE*, Matteo Buffolo, *Member, IEEE*, Francesca Rossi, Xuanqui Huang, *Member, IEEE*, Houqiang Fu, *Member, IEEE*, Hong Chen, Yuji Zhao, Andrea Gasparotto, Conny Becht, Ulrich T. Schwarz, Gaudenzio Meneghesso, *Fellow, IEEE*, Enrico Zanoni, *Life Fellow, IEEE*, and Matteo Meneghini, *Senior Member, IEEE*

***Abstract*— By combining microscopy investigation, light-beam induced current (LBIC), micro-photoluminescence (μ-PL), and micro-electroluminescence (μ-EL) characterization, we investigate the electrical and optical properties of V-pits and trench-like defects in high-periodicity InGaN/GaN multiple quantum wells (MQWs) solar cells. Experimental measurements indicate that V-pits and their complexes are preferential conductive paths under reverse and forward bias. Spectral analysis shows a redshifted wavelength contribution, with respect to MQWs emission peak wavelength, in presence of agglomerates of V-pits surrounded by trench-like defects. The intensity of the redshifted wavelength contribution is more pronounced under μ-EL with respect to μ-PL characterizations, due to the localization of carrier flow in proximity of V-defects. Results give insight on the role of V-pits and their agglomerates on the electrical and optical properties of high-periodicity quantum well structures, to be used for InGaN-based photodetectors and solar cells.**

***Index Terms*— GaN, InGaN, micro-electroluminescence (μ-EL), micro-photoluminescence (μ-PL), microscopy, multiple-quantum-well (MQW), solar cells, trench-like, V pits.**

Manuscript received 21 September 2023; revised 20 December 2023; accepted 9 January 2024. Date of publication 26 January 2024; date of current version 1 March 2024. This study was developed in the framework of the research activities carried out within the Project "Network 4 Energy Sustainable Transition—NEST", Spoke 1., Project code PE0000021, funded under the National Recovery and Resilience Plan (NRRP), Mission 4, Component 2, Investment 1.3—Call for tender No. 1561 of 11.10.2022 of Ministero dell'Università e della Ricerca (MUR); funded by the European Union—NextGenerationEU. This work was also supported by the Arizona State University and Rice University through ULTRA, an Energy Frontier Research Center (EFRC) funded by the U.S. Department of Energy, Office of Science, Basic Energy Sciences under Award DE SC0021230. The review of this article was arranged by Editor H. Nguyen. *(Corresponding author: Marco Nicoletto.)*

Marco Nicoletto is with the Department of Information Engineering, Università degli Studi di Padova, 35131 Padova, Italy (e-mail: marco.nicoletto.2@studenti.unipd.it).

Alessandro Caria, Fabiana Rampazzo, Carlo De Santi, Matteo Buffolo, Gaudenzio Meneghesso, and Enrico Zanoni are with the Department of Information Engineering, University of Padova, 35131 Padua, Italy.

Francesca Rossi is with CNR IMEM, 43124 Parma, Italy.

Xuanqui Huang, Houqiang Fu, and Hong Chen are with the School of Electrical, Computer and Energy Engineering, Arizona State University, Tempe, AZ 85287 USA.

Yuji Zhao is with the School of Electrical, Computer and Energy Engineering, Arizona State University, Tempe, AZ 85287 USA, and also with the Department of Electrical and Computer Engineering, Rice University, Houston, TX 77005 USA.

Andrea Gasparotto is with the Department of Physics and Astronomy "Galileo Galilei", University of Padova, 35131 Padua, Italy.

Conny Becht and Ulrich T. Schwarz are with the Institute of Physics, Chemnitz University of Technology, 09126 Chemnitz, Germany.

Matteo Meneghini is with the Department of Information Engineering and the Department of Physics and Astronomy, University of Padova, 35131 Padua, Italy.

Color versions of one or more figures in this article are available at https://doi.org/10.1109/TED.2024.3353711.

Digital Object Identifier 10.1109/TED.2024.3353711

I. Introduction

HIGH-PERIODICITY InGaN/GaN multiple quantum well (MQWs) devices are investigated for different applications, from concentrator solar cells [1], [2] to wireless power transfer systems [3] and space applications [4]. Such structures allow for high-efficiency light collection in the short wavelength range, thanks to their high absorption coefficient, outstanding radiation resistance, high thermal stability, and thus reliability in harsh environments [5], [6]. Until now, the research effort in improving the efficiency and reliability of InGaN MQWs solar cells has been focused on optimizing the well and barrier thickness, controlling polarization effects, and improving the material crystal quality [7], [8], [9]. However, the properties of high periodicity MQW solar cells may be significantly affected by the presence of extended defects, such as dislocations and V-pits, whose properties are still under investigation.

It is well known that during the growth of GaN devices, the difference in thermal expansion coefficient and the large lattice mismatch between GaN and sapphire substrate can lead to the formation of different structural defects such as threading dislocations (TDs), inversion domain boundaries (IDBs), basal plane stacking faults (BSFs), and stacking mismatch boundaries (SMBs) [10], [11], [12], [13]. Based on atomic force microscopy (AFM) and transmission electron microscopy (TEM), different papers reported that TDs lead to the formation of V-defects (or V-pits), which appear at the surface as open hexagonal inverted pyramid with [10], [11] side walls [14], [15], [16]. On the other hand, BSFs and

SMBs lead to the formation of trench defects, which are closed-loop boundaries with V-shaped grooves [12], [17], [18]. These extended defects may significantly worsen the optical and electrical properties of the devices and their impact on high periodicity MQW structures is still under investigation. In the literature, the influence of V-pits in the characteristics of GaN-based solar cells is more extensively investigated in PIN structures [19], [20], [21], [22], [23], focusing in their influence on the open circuit voltage (Voc) and short circuit current (Isc): an in-depth analysis of the impact of V-pits and other extended defects, such as trench-like defects, in GaN-based MQWs solar cells is missing. The goal of this article is to fill this gap, by presenting a comprehensive study based on scanning electron microscopy (SEM), light-beam-induced current (LBIC), electron-beam-induced current (EBIC), micro-electroluminescence (μ-EL), and micro-photoluminescence (μ-PL) characterization. By combining these techniques within a specific region of the device, we investigate the morphological, electrical, and optical characteristics of the defects, and describe unique features in the intensity and spectral data. First, we show that agglomerates of V-pits play a dominant role in current conduction under reverse and forward bias [24]. Second, by integrating microscopy investigation, μ-PL and μ-EL characterization, the spectral properties near different extended defects are explored in detail, by focusing on the intensity and peak wavelength dependence: a significant redshift is found in proximity of some defects, which is described through EL and PL measurements, and ascribed to the presence of trench defects.

II. Experimental Details

The high-periodicity InGaN/GaN MQWs GaN-based solar cells analyzed in this work are grown on c-plane (0001) sapphire by metal organic chemical vapor deposition (MOCVD). A schematic of the device under test is shown in Fig. 1(a). The structure consists of 2 μm silicon doped n-GaN ([Si] = 3×10^{18} cm^{-3}) layer, deposited over a sapphire substrate and a 125 nm highly silicon doped n$^+$-GaN (Si concentration [Si] = 2×10^{19} cm^{-3}) layer, to create an ohmic contact [25]. Above the n$^+$-GaN layer, the high-periodicity MQWs region is grown and is composed by 30 pairs of undoped $In_{0.15}Ga_{0.85}N$ quantum wells (well thickness = 3 nm, with an indium mole fraction of 15%) and GaN barriers (barrier thickness = 7 nm). Above the MQWs region, a 5 nm magnesium-doped p-$Al_{0.15}Ga_{0.85}N$ electron blocking layer (EBL) ([Mg] = 2×10^{19} cm^{-3}, with an aluminum mole fraction of 15%) is inserted, to enhance carrier collection at the p-side of the devices by reducing the recombination rate and increasing the carrier lifetime [25]. Above the EBL, a 150 nm magnesium doped p-GaN layer ([Mg] = 2×10^{19} cm^{-3}) is grown and finally, a 10 nm highly magnesium doped p$^+$-GaN contact layer to create an ohmic contact ([Mg] > 2×10^{19} cm^{-3}) is formed. A semi-transparent 130 nm indium-tin oxide (ITO) layer is deposited by dc-sputtering on top of the mesa as a current spreading layer with post-annealing in N_2/O_2 at 500 °C. Devices were then processed by standard lithography into 1 × 1 mm solar cells and finally, Ti/Al/Ni/Au ring contacts and Ti/Pt/Au grid contacts are deposited via electron beam evaporation around the perimeter and on the top of the mesa, respectively, to form cathode and anode. Other details of the device can be found in [25]. SEM characterization to obtain filtering grid in-beam backscattered electrons (f-BSEs) images were performed through the TESCAN SOLARIS

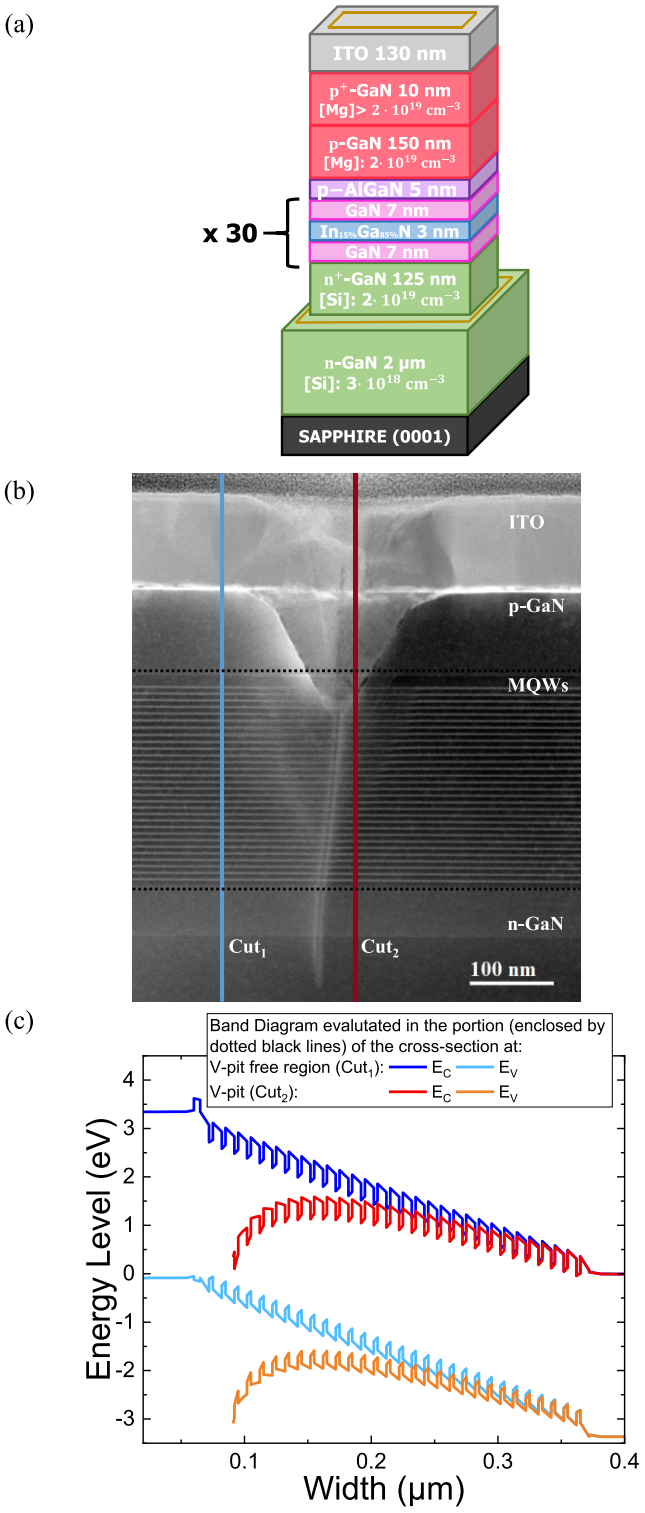

Fig. 1. (a) High-periodicity InGaN/GaN MQWs GaN-based solar cell schematic. (b) STEM image of the lateral cross section of sample with 100 nm p-GaN thickness: Cut_1 and Cut_2 line indicate where the band diagram is evaluated following the model in [24]. (c) Band diagram showing potential barrier reduction at V-defect.

microscope, which is a dual beam system containing the TriglavTM immersion optics column and the OrangeTM Ga ion optics column attached to one chamber that allows to perform surface modification using a focused ion beam (FIB). Exploiting FIB, a lamella of the analyzed device was obtained, to characterize the cross-sectional structure of the sample. The cross-sectional structure was analyzed by a TEM using a JEOL JEM-2200FS field emission microscope equipped with an in-column Ω filter, operated at 200 keV. Imaging was carried out in scanning transmission electron microscope (STEM) mode using a high-angle annular dark-field (HAADF) detector that exploits atomic-number (Z) contrast. Finally, μ-EL and μ-PL characterizations were performed through a custom designed spectral resolved confocal microscope setup which is discussed more in detail in [26], [27], and [28].

III. Characterization and Discussion

The SEM image reported in Fig. 2(a), shows the In-Beam f-BSE characterization of the analyzed area discussed in this manuscript, obtained by the TESCAN SOLARIS microscope. This area has an extension of 5×5 μm^2 and presents a high number of V-pits. V-pit formation has been ascribed to increased strain energy during GaN growth on a sapphire substrate. Other factors to take into account are a reduced Ga incorporation on the pyramid plane, a higher strain energy in high indium mole fraction in InGaN QWs and the relatively low temperatures used to grow InGaN QWs, leading to degraded GaN composition due to limited gallium surface diffusion [14], [29], [30]. In particular, in Fig. 2(a), region "r1" (red circle), region "r2" (green circle) and region "r4" (purple circle) show agglomerates of V-pits and will be reference regions for the following discussion, as well as region "r3" (light blue circle) which, unlike the previous ones, has no V-pits. The well-known open hexagonal, inverted pyramid with [10], [11] side walls shape of the V-defects is observed [31], [32], with a diagonal length in the range of 100 and 160 nm; the density of V-pits is 8.6×10^7 cm^{-2} [24].

Fig. 2(b) and (c) report the LBIC current signal measured in the same area at reverse bias (-3 V) and forward bias (2.5 V) respectively under a monochromatic 375 nm laser beam at 500 μW. Details on the μ-PL setup, including measurements of the focus spot size, is published elsewhere [26]. In these maps, the reference circles are shown to recognized reference regions ("r1," "r2" "r3" and "r4"). In Fig. 2(b), the lower value in the color scale refers to -21 mA and the higher value refers to -29 mA (relative increase of 40% in the brightest region with respect to the darkest one) while in Fig. 2(c), the lower value refers to 400 mA and the highest value refers to 412 mA (relative increase of 3%). This means that ΔI in the regions with increased current has the same sign as the bias voltage, and thus we observe an increased photocurrent for reverse bias and an increased forward current for forward bias, as observed in similar PIN GaN-based devices [19], [20], [21], [22]. In particular, from Fig. 2(b) and (c), considering the reference regions in Fig. 2(a), it is clear that agglomerates of V-pits ("r1," "r2" and "r4") are more conductive than the V-pit free region ("r3"). By comparing the images in Fig. 2, regions with V-pits and their agglomerates exhibit higher conductivity than V-pit-free regions improving the analysis and the modeling performed in our previous work [24].

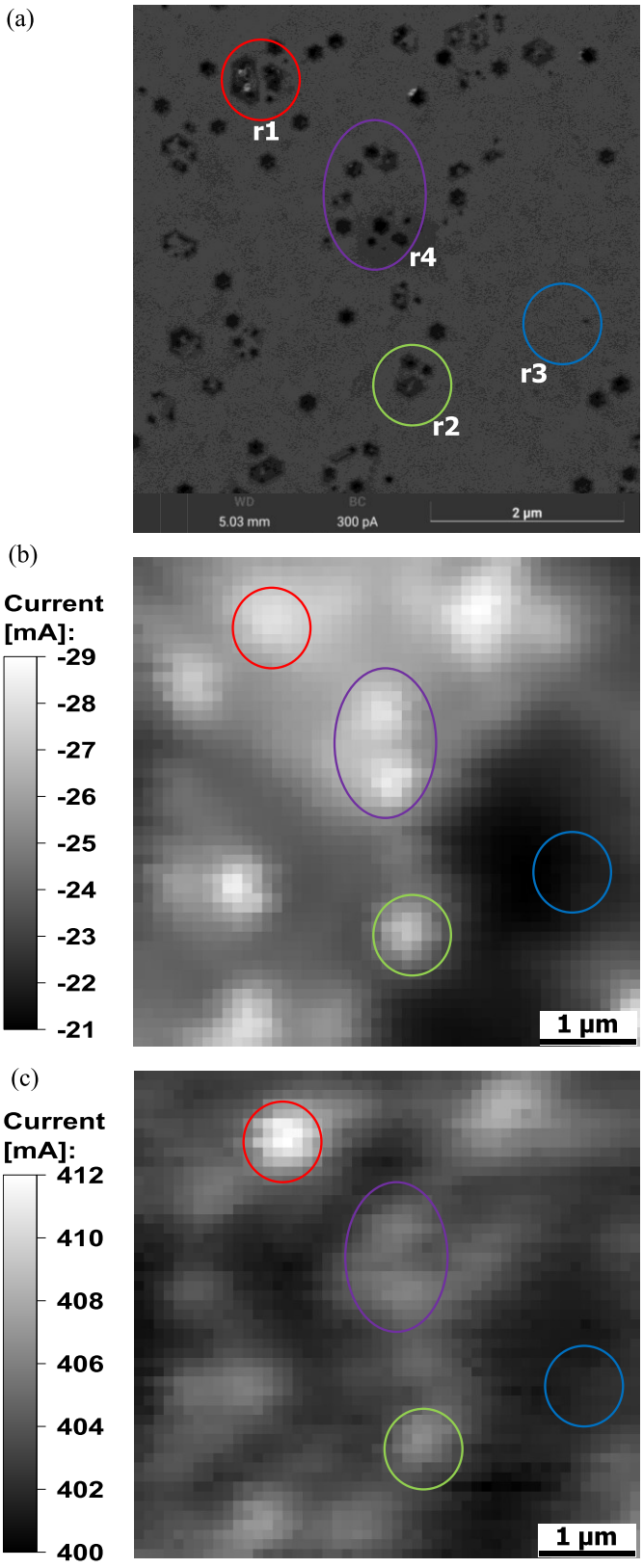

Fig. 2. 5×5 μm^2 area discussed in this work. (a) In-beam f-BSE characterization; normalized current signal in μ-PL characterization with 500 μW optical power at 375 nm. (b) Reverse bias (-3 V). (c) Forward bias (2.5 V).

The same is true also under EBIC characterization (data not shown here) where is clearly shown that V-pits and their agglomeration are more conductive than the V-pits free area. V-pits originate at the MQWs region of these device [33] and above them, layers grow differently than in the planar region where V-pits are not present, as clearly visible in the STEM image of the lateral cross section of the sample [Fig. 1(b)]. In the device under test, this results in an ITO layer, and thus the p-contact, being closer to the MQWs region resulting in the formation of localized short circuit paths with a reduced potential barrier at the p-side of the device [24] [a schematic is present in Fig. 1(c)]. Furthermore, V-pits are shown to enhance hole injection efficiency [34], [35] and feature thinner GaN barriers and lower indium concentration wells along the sidewalls [36], [37] which could constitute preferential current paths with respect to thicker barriers and deeper wells in MQWs region [38], [39], leading to a higher current signal in correspondence of V-pits and their agglomerates.

This is supported by Fig. 3, which reports the results of μ-EL analysis performed at a current injection of 80 mA. From the spectral data, measured locally, we could extract the zeroth moment μ_0, which corresponds to the integral of the spectrum and is thus proportional to the intensity of the emission

$$\mu_0 = \sum_i I_i \tag{1}$$

where I_i is the intensity signal at each wavelength λ_i and the integration runs from $\lambda = 315$–615 nm. On the other hand, the first moment μ_1 is the weighted average of the wavelength, defined as

$$\mu_1 = \frac{\sum_i \lambda_i I_i}{\mu_0} \tag{2}$$

in the same integration range as the zeroth moment. μ_1 coincides with the peak wavelength if the spectrum is symmetric, otherwise, it is a good estimation of the mean emission wavelength [27].

Fig. 3(a) and (b) show the μ-EL mapping carried out on the same 5×5 μm^2 area presenting the zeroth moment (normalized with respect to the maximum) and first moment respectively.

Considering the intensity information in Fig. 3(a) (zeroth moment), it is clear that in correspondence of agglomerates of V-pits in region "r1" and "r2," a higher intensity signal is obtained with respect to the V-pits free reference region "r3." On the other hand, the agglomerate of V-pits "r4" does not present such a high intensity signal as the other agglomerates. Taking into account the wavelength information in Fig. 3(b) (first moment), it is clear that the higher intensity value is correlated with a redshift (about 10–12 nm) of the weighted average emission wavelength. In the remaining area, the latter is uniform at a value around 450 nm.

Fig. 3(c) reports the reference spectra measured in the different regions (from "r1" to "r4"). The spectrum related to region "r4" (dotted purple line) and "r3" (blue solid line) show a peak wavelength of 447 nm which is consistent with the emission peak wavelength of devices with similar indium

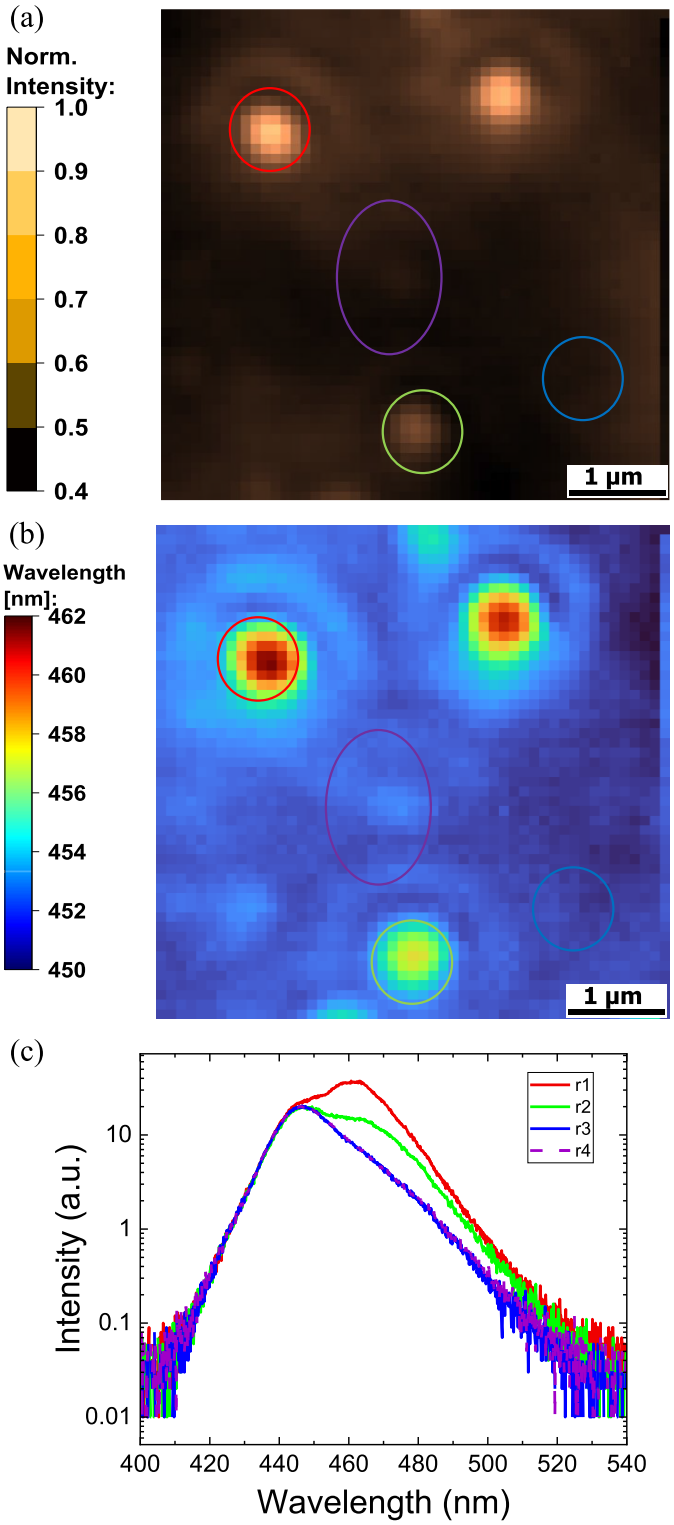

Fig. 3. μ-EL characterization of the area in Fig. 2 at 80 mA. (a) Normalized zeroth moment. (b) First moment. (c) Spectrum in "r1," "r2," "r3" and "r4."

concentration and MQWs thickness [40], [41]. On the other hand, regions "r2" (solid green line) and "r1" (solid red line) show also a peak at a redshifted wavelength of 462 nm. It is thus clear that the higher intensity in the zeroth moment arises from the occurrence of the longer wavelength contribution, which is mostly defined for agglomerates of V-pits "r1" and

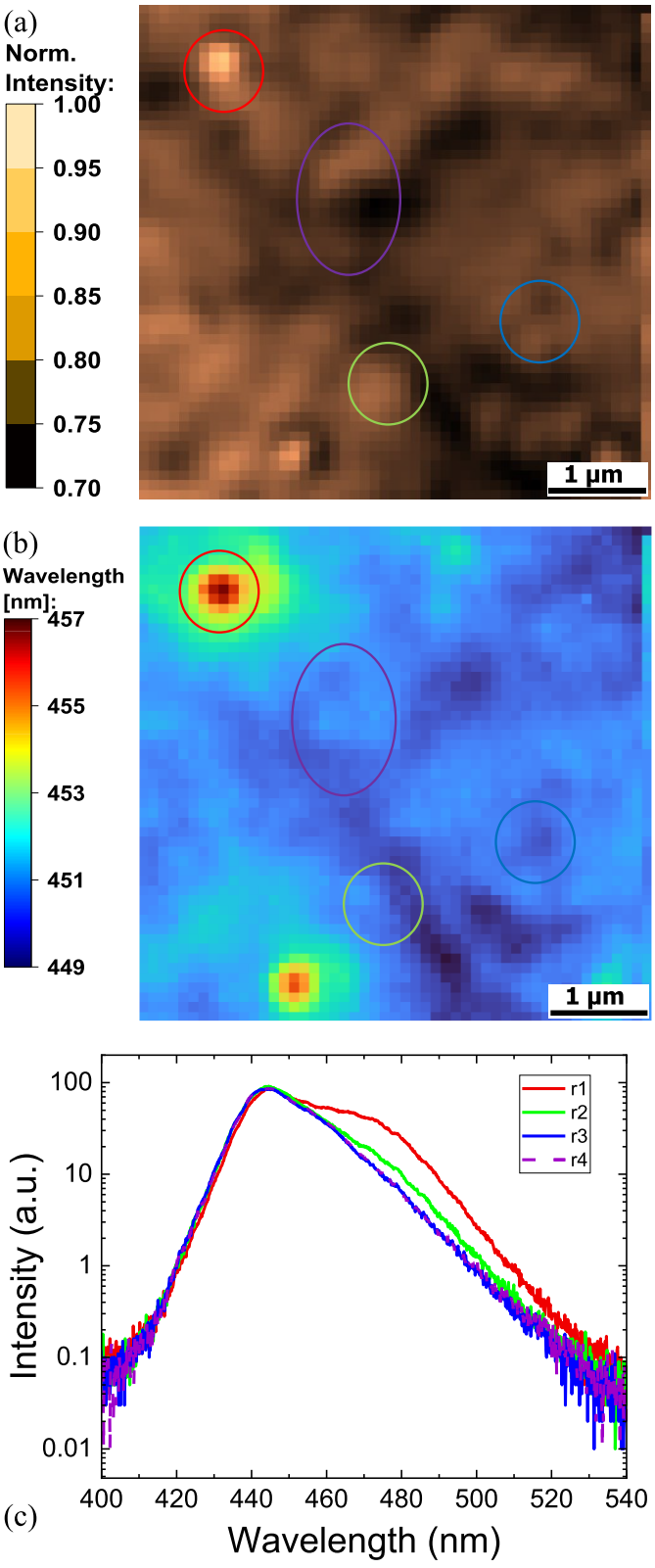

Fig. 4. μ-PL characterization of the area in Fig. 2 at 500 μW, 2 V forward bias. (a) Normalized zeroth moment. (b) First moment. (c) Spectrum in "r1," "r2," "r3" and "r4."

"r2," and absent for agglomerate "r4," which presents a similar spectrum to that of V-pits free region "r3."

Further detail was obtained by analyzing the μ-PL mapping carried out on the same 5 × 5 μm^2 area presented in Fig. 4.

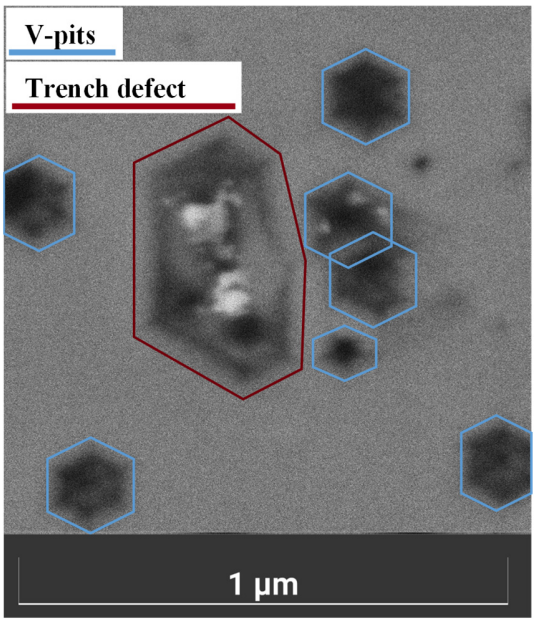

Fig. 5. High-resolution in-beam f-BSE zoom characterization of agglomeration of V-pits with trench-like defects: V-pit are surrounded by blue lines, while trench-like defect is surrounded by a red line.

Specifically, Fig. 4(a) shows the zeroth moment (normalize with respect to the maximum), Fig. 4(b) shows the first moment and Fig. 4(c) shows the spectrum in the reference regions performed at forward bias (2 V) at 500 μW optical power laser beam excitation at 375 nm (mappings are also representative of reverse bias and short circuit operation). Given the zero moment in μ-PL, the intensity is more uniformly distributed in the analyzed area with respect to μ-EL, emphasizing a lower influence of extended defects under μ-PL characterization. Also, relative amplitude of the red peak is lower in μ-PL, compared to μ-EL, achieving a more uniform emission wavelength.

Considering the first moment, reference regions "r3" and "r4" present no redshift of the weighted average wavelength with respect to the peak emission wavelength observable from the spectrum in Fig. 4(c), i.e., 447 nm (blue solid line and dotted purple line respectively).

Even reference region "r2," which shows significant redshift in first moment and significant contribution of the longer wavelength peak in the spectrum, under μ-EL characterization [Fig. 3(b)], green circle and Fig. 3(c), solid green line, shows a reduced longer wavelength contribution in the spectrum under μ-PL characterization. Only the reference region "r1" presents a high redshift in the first moment due to a significant longer wavelength peak contribution in the spectrum under both μ-EL and μ-PL characterizations [Figs. 3(b) and 4(b) red circle and Figs. 3(c) and 4(c) solid red line)].

Considering the high-resolution in-beam f-BSE zoom characterization of reference region "r1" shown in Fig. 5, it becomes clear why this region has a longer wavelength contribution in the spectrum and thus a redshift in the first moment mapping. In fact, it is possible to recognize V-pits [42], [43] (circled by a blue hexagonal line) and a trench-like defect (circled by a red line) [44]. The latter defect is found to

originate from a stacking fault lying in the basal plane (BSF), which is connected to a vertical SMB terminating at the V-shaped trenches [45]. The boundaries of the defects, made by several straight lines oriented at 60° and 120° to one other, are visible in Fig. 5 [44]. SMBs and V-pits involved in the trench-like defects are formed by relaxation, and result in an increased indium content in the region enclosed by the trench defect [44], [46]. As a consequence, a longer wavelength peak contribution in spectrum with respect to the surrounding region is observed [17], [47]. Furthermore, the difference in strain caused by the trench-like defects could favor InN migration and formation of QD structures with redshifted emission [48], [49], [50]. Additionally, with decreasing trench width, a reduced redshift and intensity is observed [45], [46] because of a narrower relaxed high-indium content region, as in the case of reference region "r2," and the region to the right of reference region "r1." Reference region "r4," instead, does not present any trench-like defects, from which no redshift weighted emission wavelength in the first moment is observed. Finally, the presence of the SMB increases the density of non-radiative recombination centers in the material, thus decreasing the quality and internal quantum efficiency of the sample [44]. A lower amount of these defects, visible through SEM, EL and PL characterization, will results in a higher efficiency and reliability of future GaN-based solar cells.

Based on the considerations above, considering that the indium concentration profile is constant throughout the MQWs region as shown by secondary-ion mass spectrometry (SIMS, data not presented here) we propose the following model to explain the related data: in μ-EL characterization, agglomerates of V-pits generate a preferential current path both for reverse photocurrent and forward current, due to the larger proximity of the p-contact to the MQWs region [24]. This results in the localization of carriers' flow and recombination near the V-pit agglomerates. In case a trench-like defect is also present (reference region "r1" and "r2"), a redshift in the first moment is observed, with respect to agglomerates of V-pits without trench (reference region "r4"), due to the increased indium content in the region enclosed by the trench defect [44], [46]. Under optical excitation, the longer wavelength peak has a lower impact, possibly due to non-radiative recombination losses at SMBs or BSFs [44], [46]. Another relevant factor is the enhanced extraction of carriers (via photocurrent) close to V-pit agglomerates [24], as confirmed by the LBIC data in reverse and forward bias.

IV. Conclusion

In conclusion, we analyzed the electrical and optical proprieties of V-pits and their agglomerates in high periodicity InGaN-GaN MQWs solar cells. First, SEM investigation combined with LBIC analysis indicate that V-pit agglomerates are preferential paths for current conduction. Second, spectral measurements indicated a significant redshift in emission wavelength in correspondence of agglomerates of V-pits surrounded by trench-like defects. Results were interpreted by considering that agglomerates of V-pits form trench-like complexes, with a stronger indium incorporation and hence a longer wavelength emission, compared to the bulk defect-free material. The results provide relevant information for the study and optimization of high periodicity MQW structures based on InGaN, for application in photodetectors and solar cells, highlighting V-pits and trench-like defects role in current conduction and spectral performance.

Acknowledgment

The views and opinions expressed are however only those of the authors and do not necessarily reflect those of the European Union or the European Commission. Neither the European Union nor the European Commission can be held responsible for them.

References

[1] R. Dahal, J. Li, K. Aryal, J. Y. Lin, and H. X. Jiang, "InGaN/GaN multiple quantum well concentrator solar cells," *Appl. Phys. Lett.*, vol. 97, no. 7, Aug. 2010, Art. no. 073115, doi: 10.1063/1.3481424.

[2] G. Moses, X. Huang, Y. Zhao, M. Auf der Maur, E. A. Katz, and J. M. Gordon, "InGaN/GaN multi-quantum-well solar cells under high solar concentration and elevated temperatures for hybrid solar thermal-photovoltaic power plants," *Prog. Photovoltaics, Res. Appl.*, vol. 28, no. 11, pp. 1167–1174, Nov. 2020, doi: 10.1002/pip.3326.

[3] C. De Santi et al., "GaN-based laser wireless power transfer system," *Materials*, vol. 11, no. 1, p. 153, Jan. 2018, doi: 10.3390/ma11010153.

[4] Y. Zhao et al., "InGaN-based solar cells for space applications," in *Proc. IEEE 60th Int. Midwest Symp. Circuits Syst. (MWSCAS)*, Aug. 2017, pp. 954–957, doi: 10.1109/MWSCAS.2017.8053083.

[5] J. Wu, "When group-III nitrides go infrared: New properties and perspectives," *J. Appl. Phys.*, vol. 106, no. 1, Jul. 2009, Art. no. 011101, doi: 10.1063/1.3155798.

[6] J. Wu et al., "Superior radiation resistance of $In_{1-x}Ga_xN$ alloys: Full-solar-spectrum photovoltaic material system," *J. Appl. Phys.*, vol. 94, no. 10, pp. 6477–6482, Oct. 2003, doi: 10.1063/1.1618353.

[7] C. J. Neufeld et al., "Effect of doping and polarization on carrier collection in InGaN quantum well solar cells," *Appl. Phys. Lett.*, vol. 98, no. 24, Jun. 2011, Art. no. 243507, doi: 10.1063/1.3595487.

[8] N. Watanabe, H. Yokoyama, N. Shigekawa, K.-I. Sugita, and A. Yamamoto, "Barrier thickness dependence of photovoltaic characteristics of InGaN/GaN multiple quantum well solar cells," *Jpn. J. Appl. Phys.*, vol. 51, no. 10S, Oct. 2012, Art. no. 10ND10, doi: 10.1143/jjap.51.10nd10.

[9] N. G. Young et al., "High-performance broadband optical coatings on InGaN/GaN solar cells for multijunction device integration," *Appl. Phys. Lett.*, vol. 104, no. 16, Apr. 2014, Art. no. 163902, doi: 10.1063/1.4873117.

[10] X. H. Wu et al., "Defect structure of metal-organic chemical vapor deposition-grown epitaxial (0001) GaN/Al_2O_3," *J. Appl. Phys.*, vol. 80, no. 6, pp. 3228–3237, Sep. 1996, doi: 10.1063/1.363264.

[11] V. Potin, P. Ruterana, G. Nouet, R. C. Pond, and H. Morkoç, "Mosaic growth of GaN on (0001) sapphire: A high-resolution electron microscopy and crystallographic study of threading dislocations from low-angle to high-angle grain boundaries," *Phys. Rev. B, Condens. Matter*, vol. 61, no. 8, pp. 5587–5599, Feb. 2000, doi: 10.1103/physrevb.61.5587.

[12] Z. Shi et al., "Formation mechanism of trench defects in green InGaN/GaN multiple quantum wells," *J. Appl. Phys.*, vol. 133, no. 12, Mar. 2023, Art. no. 123103, doi: 10.1063/5.0136104.

[13] J. S. Speck and S. J. Rosner, "The role of threading dislocations in the physical properties of GaN and its alloys," *Phys. B, Condens. Matter*, vols. 273–274, pp. 24–32, Dec. 1999, doi: 10.1016/s0921-4526(99)00399-3.

[14] X. H. Wu et al., "Structural origin of V-defects and correlation with localized excitonic centers in InGaN/GaN multiple quantum wells," *Appl. Phys. Lett.*, vol. 72, no. 6, pp. 692–694, Feb. 1998, doi: 10.1063/1.120844.

[15] H. K. Cho, J. Y. Lee, G. M. Yang, and C. S. Kim, "Formation mechanism of v defects in the InGaN/GaN multiple quantum wells grown on GaN layers with low threading dislocation density," *Appl. Phys. Lett.*, vol. 79, no. 2, pp. 215–217, Jul. 2001, doi: 10.1063/1.1384906.

[16] Y. Chen et al., "Pit formation in GaInN quantum wells," *Appl. Phys. Lett.*, vol. 72, no. 6, pp. 710–712, Feb. 1998, doi: 10.1063/1.120853.

[17] S.-L. Sahonta et al., "Properties of trench defects in InGaN/GaN quantum well structures," *Phys. Status Solidi A*, vol. 210, no. 1, pp. 195–198, Jan. 2013, doi: 10.1002/pssa.201200408.

[18] F. Shahedipour-Sandvik et al., "Origin of ring defects in high in content green InGaN/GaN MQW: An ultrasonic force microscopy study," *MRS Internet J. Nitride Semicond. Res.*, vol. 10, no. 1, p. e4, Oct. 2005, doi: 10.1557/s1092578300000557.

[19] M. Arif et al., "Role of V-pits in the performance improvement of InGaN solar cells," *Appl. Phys. Lett.*, vol. 109, no. 13, Sep. 2016, Art. no. 133507, doi: 10.1063/1.4963817.

[20] C. J. Neufeld, Z. Chen, S. C. Cruz, N. G. Toledo, S. P. DenBaars, and U. K. Mishra, "Optimization of the p-GaN window layer for InGaN/GaN solar cells," in *Proc. 35th IEEE Photovoltaic Specialists Conf.*, Jun. 2010, pp. 2089–2092, doi: 10.1109/PVSC.2010.5616061.

[21] R. M. Farrell et al., "Effect of intentional p-GaN surface roughening on the performance of InGaN/GaN solar cells," *Appl. Phys. Lett.*, vol. 103, no. 24, Dec. 2013, Art. no. 241104, doi: 10.1063/1.4844955/25975.

[22] E. Matioli et al., "High internal and external quantum efficiency InGaN/GaN solar cells," *Appl. Phys. Lett.*, vol. 98, no. 2, Jan. 2011, Art. no. 021102, doi: 10.1063/1.3540501.

[23] S. Maximenko, S. Soloviev, D. Cherednichenko, and T. Sudarshan, "Electron-beam-induced current observed for dislocations in diffused 4H-SiC $p-n$ diodes," *Appl. Phys. Lett.*, vol. 84, no. 9, pp. 1576–1578, Mar. 2004, doi: 10.1063/1.1652229.

[24] M. Nicoletto et al., "Influence of V-pits on the turn-on voltage of GaN-based high periodicity multiple quantum well solar cells," *IEEE J. Photovolt.*, vol. 13, no. 6, pp. 891–898, Nov. 2023, doi: 10.1109/JPHOTOV.2023.3311891.

[25] X. Huang et al., "Energy band engineering of InGaN/GaN multi-quantum-well solar cells via AlGaN electron- and hole-blocking layers," *Appl. Phys. Lett.*, vol. 113, no. 4, Jul. 2018, Art. no. 043501, doi: 10.1063/1.5028530.

[26] C. Becht, U. T. Schwarz, M. Binder, and B. Galler, "Diffusion analysis of charge carriers in InGaN/GaN heterostructures by microphotoluminescence," *Phys. Status Solidi B*, vol. 260, no. 8, Aug. 2023, doi: 10.1002/pssb.202200565.

[27] U. T. Schwarz, T. U. Chemnitz, M. Kneissl, T. U. Berlin, S. Gemming, and C. Deibel. (Jul. 2021). *Optical Polarization and Charge Carrier Density in Semipolar and Nonpolar InGaN Quantum Wells in Core-shell Microrods and Planar LEDs*. Accessed: Jul. 17, 2023. [Online]. Available: https://nbn-resolving.org/urn:nbn: de:bsz:ch1-qucosa2-743254

[28] C. Becht et al., "Micro-photoluminescence to investigate lateral diffusion of charge carriers in InGaN/GaN MQWs," *Proc. SPIE*, vol. 2001, Mar. 2022, Art. no. 2608901, doi: 10.1117/12.2608901.

[29] C. J. Sun et al., "Quantum shift of band-edge stimulated emission in InGaN–GaN multiple quantum well light-emitting diodes," *Appl. Phys. Lett.*, vol. 70, no. 22, pp. 2978–2980, Jun. 1997, doi: 10.1063/1.118762.

[30] I.-H. Kim, H.-S. Park, Y.-J. Park, and T. Kim, "Formation of V-shaped pits in InGaN/GaN multiquantum wells and bulk InGaN films," *Appl. Phys. Lett.*, vol. 73, no. 12, pp. 1634–1636, Sep. 1998, doi: 10.1063/1.122229.

[31] S. L. Selvaraj, A. Watanabe, and T. Egawa, "Influence of deep-pits on the device characteristics of metal-organic chemical vapor deposition grown AlGaN/GaN high-electron mobility transistors on silicon substrate," *Appl. Phys. Lett.*, vol. 98, no. 25, Jun. 2011, Art. no. 252105, doi: 10.1063/1.3602919.

[32] H. Wang, X. Wang, Q. Tan, and X. Zeng, "V-defects formation and optical properties of InGaN/GaN multiple quantum well LED grown on patterned sapphire substrate," *Mater. Sci. Semicond. Process.*, vol. 29, pp. 112–116, Jan. 2015, doi: 10.1016/j.mssp.2013.11.019.

[33] S.-W. Chen, C.-J. Chang, and T.-C. Lu, "Effect of strains and V-shaped pit structures on the performance of GaN-based light-emitting diodes," *Crystals*, vol. 10, no. 4, p. 311, Apr. 2020, doi: 10.3390/cryst10040311.

[34] S. Zhou and X. Liu, "Effect of V-pits embedded InGaN/GaN superlattices on optical and electrical properties of GaN-based green light-emitting diodes," *Phys. Status Solidi A*, vol. 214, no. 5, May 2017, Art. no. 1770125, doi: 10.1002/pssa.201770130.

[35] S. Zhou et al., "The effect of nanometre-scale V-pits on electronic and optical properties and efficiency droop of GaN-based green light-emitting diodes," *Sci. Rep.*, vol. 8, no. 1, p. 11053, Jul. 2018, doi: 10.1038/s41598-018-29440-4.

[36] I. A. Ajia et al., "Generated carrier dynamics in V-pit-enhanced InGaN/GaN light-emitting diode," *ACS Photon.*, vol. 5, no. 3, pp. 820–826, Mar. 2018, doi: 10.1021/acsphotonics.7b00944.

[37] A. M. Yong, C. B. Soh, X. H. Zhang, S. Y. Chow, and S. J. Chua, "Investigation of V-defects formation in InGaN/GaN multiple quantum well grown on sapphire," *Thin Solid Films*, vol. 515, no. 10, pp. 4496–4500, Mar. 2007, doi: 10.1016/j.tsf.2006.07.181.

[38] X. Wu et al., "Electroluminescence from the sidewall quantum wells in the V-shaped pits of InGaN light emitting diodes," *Appl. Phys. Lett.*, vol. 104, no. 22, Jun. 2014, Art. no. 221101, doi: 10.1063/1.4880731.

[39] Z. Quan, L. Wang, C. Zheng, J. Liu, and F. Jiang, "Roles of V-shaped pits on the improvement of quantum efficiency in InGaN/GaN multiple quantum well light-emitting diodes," *J. Appl. Phys.*, vol. 116, no. 18, Nov. 2014, Art. no. 183107, doi: 10.1063/1.4901828.

[40] P. Perlin et al., "InGaN/GaN quantum wells studied by high pressure, variable temperature, and excitation power spectroscopy," *Appl. Phys. Lett.*, vol. 73, no. 19, pp. 2778–2780, Nov. 1998, doi: 10.1063/1.122588.

[41] J. Yang et al., "Correlation between the structural and cathodoluminescence properties in InGaN/GaN multiple quantum wells with large number of quantum wells," *J. Vac. Sci. Technol. A, Vac., Surf., Films*, vol. 32, no. 5, Sep. 2014, Art. no. 051503, doi: 10.1116/1.4889857.

[42] M. Knetzger, E. Meissner, C. Schröter, and J. Friedrich, "Theoretical aspects and microstructural investigations on V-pit defects in HVPE grown GaN," *J. Cryst. Growth*, vol. 518, pp. 51–58, Jul. 2019, doi: 10.1016/j.jcrysgro.2019.04.012.

[43] A. N. Bright, N. Sharma, and C. J. Humphreys, "Analysis of contacts and V-defects in GaN device structures by transmission electron microscopy," *Microscopy*, vol. 50, no. 6, pp. 489–495, Nov. 2001, doi: 10.1093/jmicro/50.6.489.

[44] F. C.-P. Massabuau et al., "Morphological, structural, and emission characterization of trench defects in InGaN/GaN quantum well structures," *Appl. Phys. Lett.*, vol. 101, no. 21, Nov. 2012, Art. no. 212107, doi: 10.1063/1.4768291.

[45] J. Bruckbauer et al., "Cathodoluminescence hyperspectral imaging of trench-like defects in InGaN/GaN quantum well structures," *J. Phys. D, Appl. Phys.*, vol. 47, no. 13, Mar. 2014, Art. no. 135107, doi: 10.1088/0022-3727/47/13/135107.

[46] F. C. P. Massabuau et al., "Correlations between the morphology and emission properties of trench defects in InGaN/GaN quantum wells," *J. Appl. Phys.*, vol. 113, no. 7, Feb. 2013, Art. no. 073505, doi: 10.1063/1.4792505.

[47] G. Kusch et al., "Carrier dynamics at trench defects in InGaN/GaN quantum wells revealed by time-resolved cathodoluminescence," *Nanoscale*, vol. 14, no. 2, pp. 402–409, 2022, doi: 10.1039/d1nr06088k.

[48] J. Bruckbauer, P. R. Edwards, T. Wang, and R. W. Martin, "High resolution cathodoluminescence hyperspectral imaging of surface features in InGaN/GaN multiple quantum well structures," *Appl. Phys. Lett.*, vol. 98, no. 14, Apr. 2011, Art. no. 141908, doi: 10.1063/1.3575573.

[49] J.-Y. Chung et al., "Light-emitting V-pits: An alternative approach toward luminescent indium-rich InGaN quantum dots," *ACS Photon.*, vol. 8, no. 10, pp. 2853–2860, Oct. 2021, doi: 10.1021/acsphotonics.1c01009.

[50] T. Vaněk et al., "Luminescence redshift of thick InGaN/GaN heterostructures induced by the migration of surface adsorbed atoms," *J. Cryst. Growth*, vol. 565, Jul. 2021, Art. no. 126151, doi: 10.1016/j.jcrysgro.2021.126151.

Open Access funding provided by 'Università degli Studi di Padova' within the CRUI-CARE Agreement